ADVANCED QUANTUM TECHNOLOGIES
www.advquantumtech.com

Coherent Swing-Up Excitation for Semiconductor Quantum Dots

Katarina Boos, Friedrich Sbresny, Sang Kyu Kim, Malte Kremser, Hubert Riedl, Frederik W. Bopp, William Rauhaus, Bianca Scaparra, Klaus D. Jöns, Jonathan J. Finley, Kai Müller, and Lukas Hanschke*

Developing coherent excitation methods for quantum emitters ensuring high brightness, optimal single-photon purity and indistinguishability of the emitted photons has been a key challenge in the past years. While various methods have been proposed and explored, they all have specific advantages and disadvantages. This study investigates the dynamics of the recent swing-up scheme as an excitation method for a two-level system and its performance in single-photon generation. By applying two far red-detuned laser pulses, the two-level system can be prepared in the excited state with near-unity fidelity. The successful operation and coherent character of this technique are demonstrated using a semiconductor quantum dot (QD). Moreover, the multi-dimensional parameter space of the two laser pulses is explored to analyze its impact on excitation fidelity. Finally, the performance of the scheme as an excitation method for generating high-quality single photons is analyzed. The swing-up scheme itself proves effective, exhibiting nearly perfect single-photon purity, while the observed indistinguishability in the studied sample is limited by the influence of the inevitable high excitation powers on the semiconductor environment of the quantum dot.

1. Introduction

Semiconductor quantum dots (QDs) are among the most promising candidates for applications in photonic quantum technologies.[1,2] They are under close investigation as a material system for optically-active spin qubits for photonic quantum gates,[3] remote-entanglement,[4,5] or the generation of highly-entangled photon graph states.[6,7] Furthermore, especially as single-photon sources they outperform other solid-state quantum emitters in terms of brightness and quality of the emitted photons.[8–12] For the generation of single photons, in recent years many resonant and non-resonant methods for excitation have been established, such as cross-polarized resonant excitation,[13,14] phonon-assisted excitation,[15–17] excitation via the p-shell,[18,19] dichromatic excitation,[20,21] or excitation via the biexciton.[11,22,23] Even though each of these methods is promising in its own way, they come along with specific individual disadvantages. For example, resonant excitation requires challenging filtering,[24–26] while non-resonant excitation introduces additional timing-jitter which limits the indistinguishability of the emitted photons.[27,28] Other limitations of some of the schemes are low efficiency or simply the restriction to a specific level scheme like the presence of a cascaded level structure.[11,29] Moreover, for applications where the coherence of the system has to be maintained, coherent excitation is crucial. Recently, Bracht et al.[30] proposed a promising technique which combines coherent and off-resonant excitation for a two-level system, whose principle functionality

K. Boos, F. Sbresny, S. K. Kim, W. Rauhaus, B. Scaparra, K. Müller
Walter Schottky Institut
TUM School of Computation
Information and Technology, and MCQST
Technische Universität München
Am Coulombwall 4, 85748 Garching, Germany
E-mail: katarina.boos@wsi.tum.de

M. Kremser, H. Riedl, F. W. Bopp, J. J. Finley
Walter Schottky Institut
TUM School of Natural Sciences, and MCQST
Technische Universität München
Am Coulombwall 4, 85748 Garching, Germany

K. D. Jöns, L. Hanschke
Institute for Photonic Quantum Systems (PhoQS)
Center for Optoelectronics and Photonics Paderborn (CeOPP) and
Department of Physics
Paderborn University
Warburger Str. 100, 33098 Paderborn, Germany

The ORCID identification number(s) for the author(s) of this article can be found under https://doi.org/10.1002/qute.202300359

DOI: 10.1002/qute.202300359

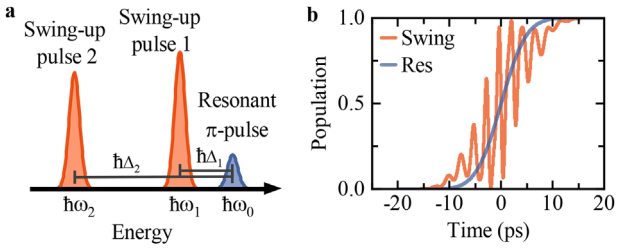

Figure 1. Schematic illustration and simulation of the swing-up excitation. a) Qualitative energy separation of the far red-detuned pulses for swing-up excitation (orange) and the resonant pulse (blue). b) Simulated time-resolved state occupation for swing-up (orange) and resonant π-pulse population inversion (blue) during the excitation process.

was confirmed experimentally by Karli et al.[31] This swing-up excitation method is based on two far red-detuned laser pulses which swing up the population from ground to excited state for a specific relation in their multi-dimensional space—frequency, intensity, pulse duration, and timing. This elegant way of exciting the two-level system directly is highly promising as the theoretical model predicts near-unity population inversion and good quality of the emitted photons while enabling frequency filtering and high brightness.

In this work, we explore the swing-up excitation method experimentally and theoretically with regard to the multi-dimensional parameter space. We find several resonances and good agreement between our experimental results and numerical simulations. Furthermore, we compare the characteristics of the emitted photons to the ones generated via resonant excitation in terms of lifetime, single-photon purity and indistinguishability.

2. Results

2.1. Swing-Up Excitation Scheme

In our study, the two-level system is realized by the transition of the negatively charged exciton in a QD, with one single electron e^- in the QD as the ground state $|0\rangle$ and the trion X^- as the excited state $|1\rangle$. The transition energy between excited and ground state is given by $\hbar\omega_0$ while the laser energies are given by $\hbar\omega_i = \hbar\omega_0 + \hbar\Delta_i$ with $i = 1, 2$, where $\hbar\Delta_i$ is the detuning from resonance, and Δ_i is negative. The system can be easily inverted from $|0\rangle$ to $|1\rangle$ with near-unity efficiency under resonant excitation with a π-pulse area as schematically illustrated in blue in **Figure 1b**.[32] While a single red-detuned laser pulse with $\hbar\Delta < 0$ is incapable of efficiently transferring population, certain combinations of two red-detuned pulses enable near-unity population inversion.[30] For the swing-up scheme, the system Hamiltonian in the rotating frame oscillating at the center frequency of the less detuned laser pulse and after applying the rotating wave approximation is

$$H = -\hbar\Delta_1\sigma^\dagger\sigma + \frac{1}{2}\hbar(\Omega^*(t)\sigma + \Omega(t)\sigma^\dagger) \quad (1)$$

where the two-color excitation field is described by

$$\Omega(t) = \Omega_1(t) + \Omega_2(t+\tau)e^{-i(\omega_2-\omega_1)t} \quad (2)$$

with Gaussian envelopes $\Omega_i(t)$ and time delay τ between the pulses. The integrated pulse areas are given by $\alpha_i = \int_{-\infty}^{+\infty}\Omega_i(t)\,dt$. The excitation pulses are schematically depicted in Figure 1a in orange. Note that the phase between the pulses does not affect the scheme and is thus set to zero.[30] By solving the von Neumann equation $\frac{\partial}{\partial t}\rho(t) = -\frac{i}{\hbar}[H, \rho(t)]$ where ρ is the density matrix, we can calculate the population of the excited state.[30] Details on the simulations are discussed in the Supporting Information.[33] As shown by the simulation results in Figure 1b in orange, the population can be inverted with near-unity fidelity, where the occupation is not smoothly transferred but shows an oscillatory, up-swinging behaviour during the presence of the pulse. Intuitively, population inversion by the swing-up scheme can be understood in the dressed-state picture. The first close-detuned pulse dresses the states, while the second pulse resonantly drives transitions within these new states.[34] For our measurements, we used a single InGaAs QD embedded in a Schottky diode structure. The diode stabilizes the charge environment in the vicinity of the QD and enables deterministic switching between neutral and negatively charged QD ground states.[35,36] A distributed Bragg reflector beneath the QD layer enhances the collection efficiency while forming a weak cavity with the sample surface. The sample is cooled down to 4.2K in a dip-stick cryostat. Further information on sample and experimental setup can be found in Section 4.

2.2. Exploration of the Excitation Parameter Space

To identify for which combination of parameters the population inversion is successful, we monitor the emission intensity of the trion transition while changing different pulse parameters of the swing-up excitation. As the parameter space is multi-dimensional, we record 2D colormaps as presented in **Figure 2** where we scan the detuning and the laser intensity of the second laser pulse to find resonances and characteristics of the system, while we vary another third parameter from map to map. The integrated trion emission is normalized to the maximal intensity of the specific parameter set for better visibility in each map. As a first step we keep the pulse lengths at 10 ps and fix the detuning and intensity of the first pulse to $\hbar\Delta_1 = -0.7$ meV and $\alpha_1 = 8\pi$, respectively. The intensity of the pulse is normalized to the power of a resonant pulse with an area of, 1π determined from resonant Rabi oscillations. We scan the detuning and the intensity of the second laser pulse in the range where high population inversion is to be expected;[30] from $\hbar\Delta_2 = -3$ meV to -0.92 meV and from $\alpha_2/\alpha_1 = 0.44$ to 1.81. Results can be seen in Figure 2a with both experimental data (left) and simulations (right) in good agreement. One main region of high excitation fidelity can be seen at around $\hbar\Delta_2 = -2$ meV, slightly shifting toward larger detunings with higher intensity. Within, we find a maximal population inversion at $\alpha_2/\alpha_1 = 1.1$ and $\hbar\Delta_2 = -2.05$ meV, indicated by the black mark, and estimate the fidelity $F_{exp} = \frac{I_{int,swing}}{I_{int,res,1\pi}}$, the ratio of emission intensity under swing-up excitation to that under a resonant π-pulse excitation which is typically in the low nW regime, to 0.66. Notably, simulations suggest a maximum attainable efficiency of 0.97 for similar parameters. The reduced efficiency in the experiment is most likely to originate from laser-induced dephasing, loss of charge carriers by interaction of the laser light field with defects and free electrons, and uncertainties such as

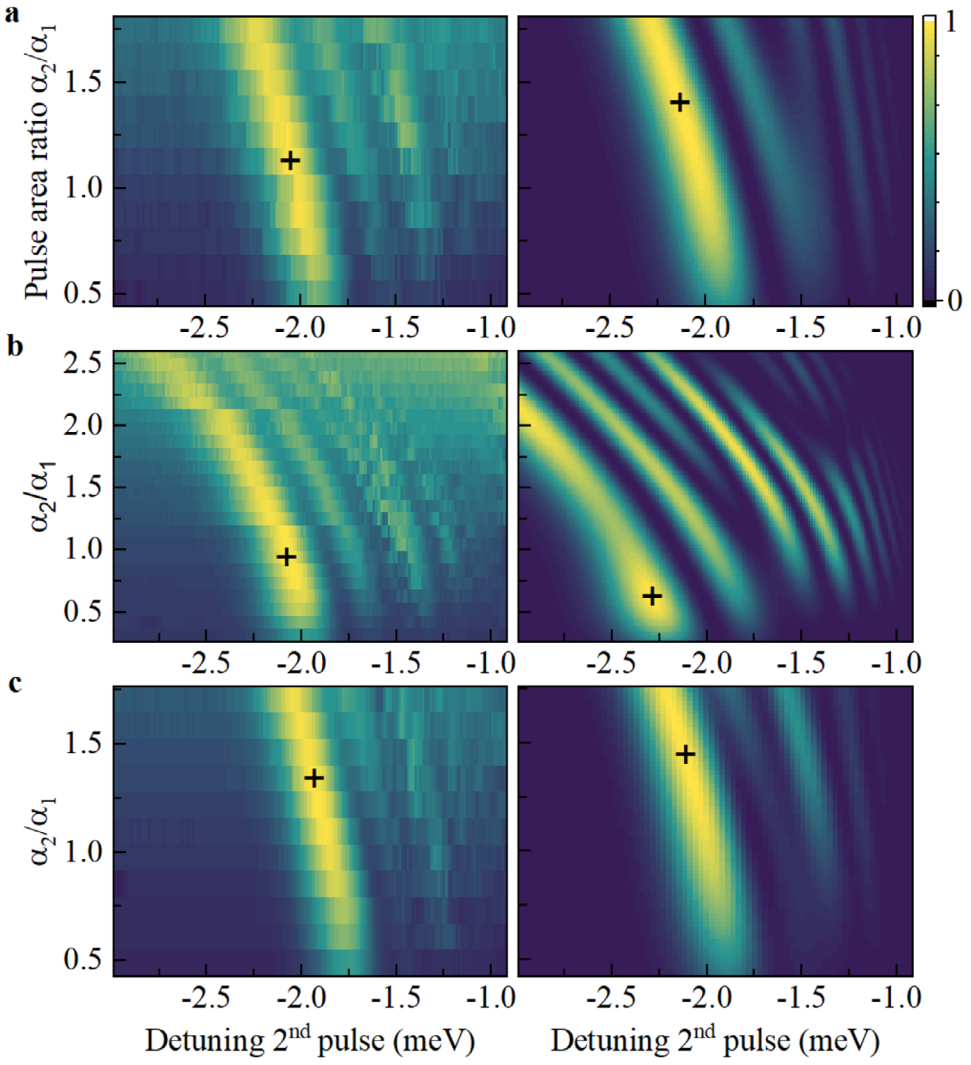

Figure 2. Normalized trion emission intensity plotted as a two-dimensional colormap in dependence of detuning and intensity of the second pulse given in terms of pulse area ratio α_2/α_1, each with fixed parameters for the first laser and for pulse length of 10 ps. Both experimental data (left) and simulations (right) are shown. First laser at a) $\hbar\Delta_1 = -0.7$ meV and $\alpha_1 = 8\pi$, b) $\hbar\Delta_1 = -0.7$ meV and $\alpha_1 = 11\pi$, and c) $\hbar\Delta_1 = -0.7$ meV and $\alpha_1 = 8\pi$ with a 4 ps time delay for the second laser. Resonances can be observed with clear maxima revealing population inversions up to 0.67 in the experiment. Each parameter set with the maximal population inversion is marked by a black cross.

deviation in pulse shape, power fluctuations and birefringence. Toward lower detunings, additional weaker resonances can be seen. These clear oscillations in intensity over a wide detuning range indicate the coherent nature of the swing-up excitation and confirm that the emission does not originate from one of the laser pulses alone. In order to see the impact of the intensity of the first laser pulse, we now increase α_1 to 11π (Figure 2b). While the signatures are similar to the lower-intensity case, their structure is more complex and features more resonances. In the experiment, we reach a similar efficiency of 0.67 with $\alpha_2/\alpha_1 = 0.93$ and $\hbar\Delta_2 = -2.08$ meV while the simulated efficiency goes up close to 1.00 (both marked in black). However, a minor mismatch between simulation and experiment can be observed: in the simulation, the regions of high intensity are shifted to larger negative detunings of the second laser with respect to the measured data. This shift increases as the pulse area of the second pulse is increased. In addition, multiple maxima appear in the simulated data set which are absent in the measured data. This small deviation between simulations and experiment is likely to result from a wavelength-dependent coupling of the detuned lasers to the weak cavity of the sample, forming between the distributed Bragg reflector beneath the QD and the sample surface. Since the power of the detuned lasers is calibrated to the pulse area needed for a resonant Rabi oscillation, a wavelength-dependent coupling of the laser leads to a small error in the pulse area, which due to the non-linear shift of the swing-up resonances results in small differences in the colormaps. For high pulse areas in a region where $\alpha_2/\alpha_1 \in [2, 2.5]$ and small detuning $\hbar\Delta_2 < -5$ meV we observe a background, that is, emission of the X^- transition independent of the detuning of the second laser. The background implies non-coherent excitation induced by the high laser intensities in the μ W regime, for example, excitation by

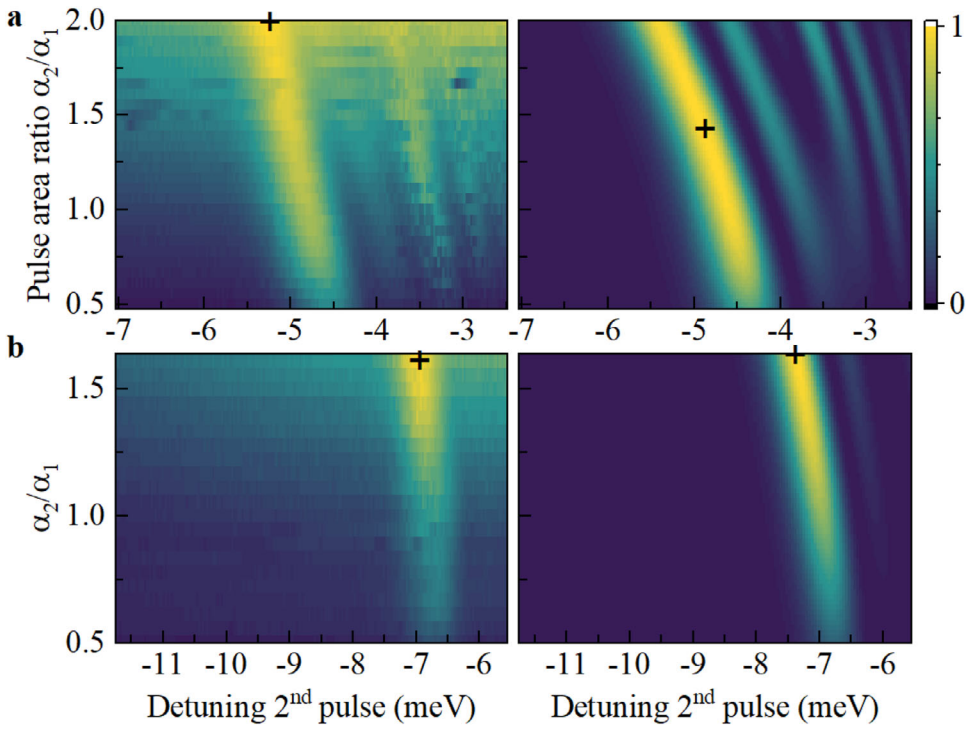

Figure 3. Experimental (left) and simulated (right) swing-up excitation fidelity dependent on detuning and intensity of the second pulse for fixed parameters of the first pulse at 5 ps pulse duration. First laser is centered at a) $\hbar\Delta_1 = -1.65$ meV and $\alpha_1 = 9\pi$, b) $\hbar\Delta_1 = -3$ meV and $\alpha_1 = 9\pi$. With increasing detuning, the areas of highest population inversion with its maxima marked with black crosses are shifted toward higher excitation intensity.

phonon-absorption, and thus, for investigating the quality of the emitted photons using lower laser intensities is beneficial. Note that on the other hand too low pulse intensity decreases the efficiency of the scheme, making it challenging to find an optimal parameter set for the studied sample.[33] To further explore the multi-dimensional swing-up parameter space, we now turn to the effect of the time delay between the two pulses, for which we delay the second pulse by 4 ps with respect to the first one (Figure 2c). Consistent with the simulations, we see that the general characteristics of the swing-up excitation do not change much for an additional delay of 4 ps, that is, we find the highest population efficiency to be 0.61 at $\alpha_2/\alpha_1 = 1.33$ and $\hbar\Delta_2 = -1.94$ meV in the experiment, and a fidelity of 0.95 in theory, which is similar to the maxima without delay. This is beneficial for applications that use this technique as it proves robust to fluctuations in the timing of the two pulses. Simulations show that the excitation works efficiently as long as the two pulses have a significant overlap[33] while being symmetric with respect to positive and negative delay.[30] It is worthwhile to note that Bracht et al. suggest that with zero time delay a maximal fidelity of 0.90 can be achieved and a pulse separation of 2.5 ps would achieve the highest population inversion for their studied pulse parameter set,[30] while simulations with our experimental parameter set show that unity population inversion could be achieved with zero delay.

To continue the study of the phase space, we investigate shorter pulses, that is, 5 ps on a second QD. Experimental results and simulation with the first laser at $\hbar\Delta_1 = -1.65$ meV and $\alpha_1 = 9\pi$ can be seen in **Figure 3a** and show good agreement and similar resonances as for longer pulses. Note that the power of the resonant π-pulse to which the intensities are normalized is higher by a factor of 3 compared to the power for the 10 ps pulses due to their decreased spectral overlap with the narrow QD transition. In agreement with the measurements performed with higher excitation intensities (Figure 2), high laser power induces a discrepancy between the resonance lines of experiment and simulation. In addition, in the experiment the point of highest occupation appears to be shifted toward higher pulse intensities, that is, to a point above $\alpha_2/\alpha_1 = 2.0$ which is outside of the measured region and where the emission background between the resonance lines is non-negligible. In Figure 2a, the experimentally observed highest fidelity of 0.80 at $\alpha_2/\alpha_1 = 2.00$ and $\hbar\Delta_2 = -5.24$ meV in the scanned region, as marked in black, contains much of the non-resonantly excited background emission, such that we can only see it as an upper bound. The theoretical maximum of close to 1.00 is shifted to lower intensity. Compared to excitation with 10 ps pulses, we see that the maximum population inversion is strongly shifted toward higher detunings and higher intensities of the second laser which is experimentally challenging and requires further engineering of the sample design. Furthermore, there are higher constraints for shorter pulses as larger detunings are required to prevent spectral overlap with the fundamental transition and as the short pulse duration leads to a higher impact of the relative pulse delay. Increasing the detuning of the first laser pulse (Figure 3b) while keeping all other parameters constant results in fewer resonances that shift to higher detuning of the second laser as predicted by theory.[30] The experimentally observed maximum of 0.40 at $\alpha_2/\alpha_1 = 1.61$ and $\hbar\Delta_2 = -6.95$ meV and the theoretical highest fidelity of 0.68 seem not to

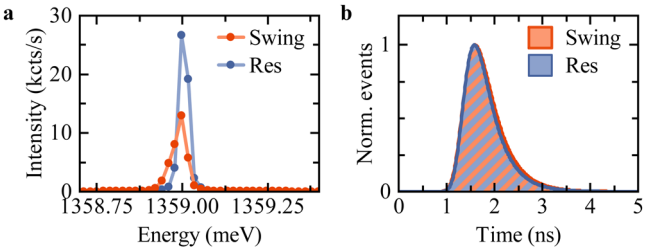

Figure 4. Emission spectra a) and radiative lifetime b) of the trion transition under swing-up excitation (orange) compared to resonant excitation (blue). The emission peak under swing-up excitation is slightly broadened and shifted due to effects of the high laser intensities on the surrounding solid-state environment. The radiative lifetimes of emission under both excitation methods are comparable.

represent the highest fidelity for the respective resonances, as they are on the edge of the measured region. However, from the simulations, it can be observed that the maximal occupation is shifted to higher powers, which can not be confirmed experimentally as the area of maximal occupation is shifted outside of the measured region. Taken together, for the studied sample we find a trade-off between best efficiency and minimal background at a fidelity of 0.67 with the first pulse set to $\hbar\Delta_1 = -0.7$ meV and $\alpha_1 = 11\pi$, and the second pulse set to $\alpha_2/\alpha_1 = 0.94$ and $\hbar\Delta_2 = -2.08$ meV for 10 ps pulses corresponding to the maximum in Figure 2b.

2.3. Single-Photon Properties

Having found optimal parameters for the excitation technique and sample under investigation we now proceed to characterize the quality of the single photons emitted from the QD under swing-up excitation. To benchmark the characteristics, we compare the results with emission under the established coherent resonant excitation.

To gain initial insight into the quality of the swing-up photons, we take a look at the emission spectrum taken with a spectrometer (**Figure** 4a, orange line). Compared to the emission peak under resonant excitation (Figure 4a, blue line) the integrated intensity is reduced to 0.67, showing the lower efficiency of the excitation method. However, note that the measurements were taken in a setup where the emitted light in the detection path is filtered by a linear polarizer, reducing the intensity by 0.5 overall. This is needed for the measurements with resonant excitation to separate QD emission and excitation laser while it would not be necessary for the excitation via swing-up due to spectral detuning of excitation and emission. This experimentally achieved inversion efficiency is lower compared to previous work,[31] where similar emission intensity under swing-up and two-photon excitation are observed. Two more observations can be made comparing the emission to the one under resonant excitation: The spectrum is shifted by about 11μ eV and slightly broadened. We attribute this to a susceptibility of the semiconductor environment to the detuned but strong laser pulses required for swing-up excitation, that is, by unintended generation of charge noise. To verify this, we analyze the X^- emission under phonon-assisted excitation and the X^{0C} emission of the biexciton cascade under two-photon excitation with increasing excitation power. In both cases we observe similar characteristics (Supporting Information[33]). The shift can be explained by re-normalization of the resonance due to localized heating of the material, while the broadening can be attributed to spectral diffusion induced by the strong laser pulses. Nevertheless, as both artifacts increase with laser power, we aim to stay at low excitation powers to ensure a high quality of the emitted photons. Time-resolved photoluminescence measurements of both swing-up and resonant excitation are presented in Figure 4b and confirm comparable values of the lifetimes of 450 ± 14 ps and 419 ± 13 ps, respectively. This similarity in excited-state lifetime rules out unexpected effects related to the swing-up excitation process and confirms the picosecond timescale of the excitation.

To study the single-photon purity we measure the second-order correlation function $g^{(2)}(\tau)$. The time-resolved correlations are presented in **Figure** 5a, yielding a raw value of $g^{(2)}(0)_{\text{swing,raw}} = 0.033 \pm 0.001$ for swing-up excitation (orange). Taking the background of the SPADs into account (Supporting Information[33]), we achieve a corrected value of $g^{(2)}(0)_{\text{swing, corr}} = 0.013 \pm 0.001$ which is so far the lowest $g^{(2)}(0)$ value for swing-up excitation, likely due to the optimized excitation conditions. This is in excellent agreement with the raw value of $g^{(2)}(0)_{\text{res,raw}} = 0.031 \pm 0.001$ and background-corrected value of $g^{(2)}(0)_{\text{res,corr}} = 0.016 \pm 0.001$ for resonant excitation (Figure 5a right), implying that there are no limitations on the single-photon purity from the swing-up scheme itself. The limiting factor for the single-photon purity in this case is the re-excitation which is especially relevant for excitation pulses which are long with respect to the radiative lifetime.[37]

We conclude our investigation of the quality of the emitted single photons with the study of their indistinguishability. To this end, we measure correlations of consecutively emitted photons in an unbalanced Mach-Zehnder interferometer. The correlation histogram for photons under swing-up excitation is depicted in Figure 5b on the left. Evaluating the Hong-Ou-Mandel-visibility ν_{HOM} by comparing the center peak to the neighbouring peaks (Supporting Information[33]) we obtain a value of $\nu_{\text{HOM,swing}} = 0.439^{+0.047}_{-0.049}$ which, to the best of our knowledge, is the first measured indistinguishability for photons emitted by a QD under swing-up excitation. This is lower than the value of $\nu_{\text{HOM,res}} = 0.663^{+0.032}_{-0.035}$ obtained for resonant excitation. We attribute this degradation under swing-up excitation to the broadened emission peak and thus decreased spectral overlap caused by the high laser intensities. A negligible time-dependent intensity fluctuation between the two detectors in the HOM measurement indicates that the limited efficiency of 0.67 of the excited state population comes from a statistical mixture rather than a pure superposition state, confirming that the observed limited fidelity originates from dephasing induced by the high laser powers.[33,38] We note that for our sample and resonant excitation, the indistinguishability of trion emission is reduced compared to the neutral exciton emission which yields $\nu_{\text{HOM,res},X^0} = 0.821^{+0.019}_{-0.018}$,[33] indicating the presence of co-tunneling between the QD and the n-doped layer. However, using swing-up excitation with uncharged QDs adds further complexity due to the overlap of swing-up resonances of the neutral exciton and two-photon swing-up resonances of the biexciton. Consequently, to exploit the full potential of the swing-up excitation further optimized samples are required which exhibit less co-tunneling and less spectral diffusion

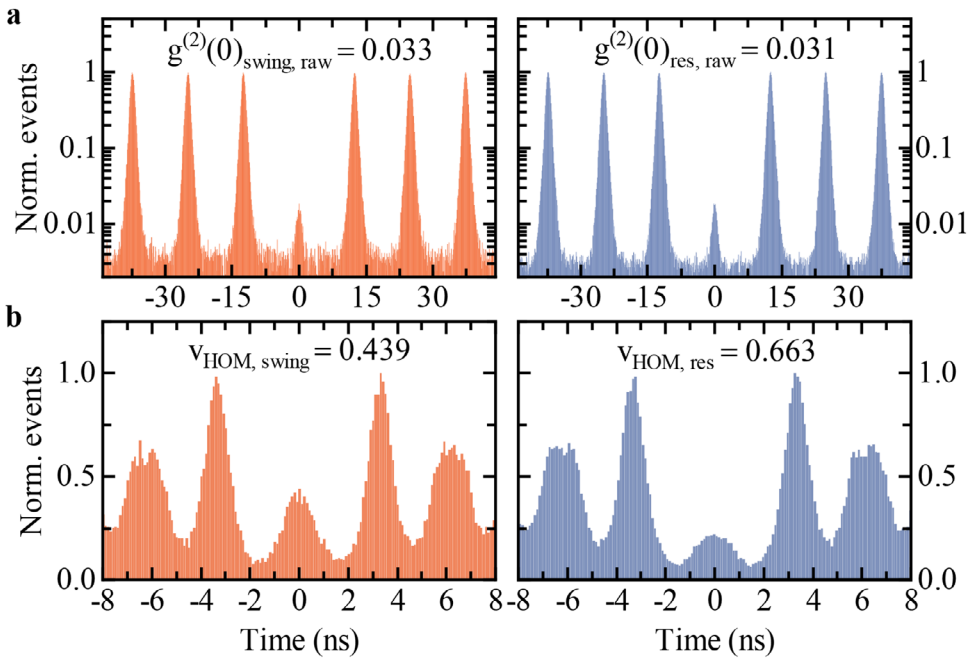

Figure 5. Single-photon purity and indistinguishability of single photons emitted under swing-up excitation. a) Second-order correlation function/histogram of swing-up excitation (orange) and resonant excitation (blue). Both raw values of $g^{(2)}(0)_{\mathrm{swing,raw}} = 0.033 \pm 0.001$ and $g^{(2)}(0)_{\mathrm{res,raw}} = 0.031 \pm 0.001$ are in excellent agreement. b) Correlation measurements of the swing-up excitation (orange) show a visibility of $v_{\mathrm{HOM,swing}} = 0.439^{+0.047}_{-0.049}$ which is lower than the value of $0.663^{+0.032}_{-0.035}$ obtained for resonant excitation (blue). This is attributed to the spectral broadening of the emission observed in Figure 4.

resulting from detuned but strong laser pulses. Such improvements can be realized by embedding the QD in a cavity structure, that is, a broad-band bullseye cavity or a planar microcavity, to enhance light-matter coupling,[39] thereby decreasing the required excitation intensities and increasing the brightness. Furthermore, a pin-diode replacing the Schottky diode could reduce noise related to trapping of laser-induced free charge carriers at the metal-semiconductor interface of the Schottky diode.

3. Discussion and Conclusion

In summary, we have investigated the recent swing-up excitation method[30] in detail by studying the multi-dimensional parameter space spanned by the two laser pulse parameter sets with respect to feasibility in the experiment and the quality of the emitted single photons. The scheme is very promising as it uses two far red-detuned laser pulses for a coherent population transfer due to beating of the frequencies with predicted near-unity fidelity. In general, the excitation method works well with up to 0.67 efficiency compared to a resonant 1π pulse within a certain parameter range that is currently fixed by experimental limitations. We find a near-perfect single-photon purity with $g^{(2)}(0)_{\mathrm{swing,corr}} = 0.013 \pm 0.001$. In addition, we measured the indistinguishability yielding a value of $v_{\mathrm{HOM,swing}} = 0.439^{+0.047}_{-0.049}$ which is limited by the studied sample, in particular by co-tunnelling and spectral diffusion caused by the high laser powers. However, with optimized samples we anticipate the scheme to contribute significantly to the generation of complex non-classical states of light, such as photonic graph states, which require a combination of coherent excitation, high brightness, high indistinguishability, and absence of polarization filtering.

4. Experimental Section

Theoretical Model: In the simulations, a two level system consisting of a ground state $|0\rangle$ and an excited state $|1\rangle$ with an energy separation between the two states of $\hbar\omega_0$ and a bichromatic driving field $E(t)$ were considered within the rotating wave approximation. Assuming that the field is linearly polarized in x-direction, a time-dependent term $\Omega(t) = -d_x E(t)/\hbar$ is defined, where d_x is the transition dipole moment in x-direction. The total excitation field consisting of two independent Gaussian pulses is given by

$$\Omega(t) = \Omega_1(t)e^{-i\omega_1 t} + \Omega_2(t+\tau)e^{-i\omega_2 t + i\phi} \tag{3}$$

where $\omega_{1,2}$ are the center frequencies of the two pulses, τ and ϕ are time delay and phase difference between the two pulses, respectively. Note that the phase does not affect the scheme and is neglected for further calculations.[30] Real Gaussian pulse envelopes $\Omega_{1,2}(t)$ are given by $\alpha_{1,2}/\sqrt{2\pi\sigma_{1,2}^2}\,\exp[-t^2/(2\sigma_2^{1,2})]$, where $\sigma_{1,2} = \mathrm{FWHM}_{1,2}/\sqrt{4\ln 2}$ are described by the intensity full width half maximum ($\mathrm{FWHM}_{1,2}$) of each pulse, and $\alpha_{1,2}$ are pulse areas defined by $\alpha_{1,2} = \int_{-\infty}^{+\infty}\Omega_{1,2}(t)\,dt$. Thus the system Hamiltonian can be described by

$$H = \hbar\omega_0\sigma^\dagger\sigma + \frac{\hbar}{2}\Omega(t)\left(\sigma + \sigma^\dagger\right) \tag{4}$$

where the annihilation operator of the two level system is defined by $\sigma = |0\rangle\langle 1|$. For further calculations, the rotating wave approximation is applied and move to the frame rotating at the center frequency of the closer

detuned laser pulse. To study the dynamics and the final population in the excited state, the Von-Neumann equation is solved

$$\frac{\partial}{\partial t}\rho(t) = -\frac{i}{\hbar}[H,\ \rho(t)] \tag{5}$$

within the time range from t_i to t_f. The time-dependent density operator $\rho(t)$ is initialized in the ground state, that is, $\rho(t_i) = |0\rangle\langle 0|$. The final excited state population is calculated as $\langle 1|\,\rho(t_f)\,|1\rangle$. For the calculations, a finite time window of 80 ps exceeding the time of the population inversion is used.

Sample Structure: The sample used for the measurements consists of self-assembled InGaAs QDs grown by molecular beam epitaxy. The layer of dots are enclosed by a diode to further control and stabilize the environment,[35,36] while a distributed Bragg reflector beneath the QDs enhances the collection efficiency. The distributed Bragg reflector forms a weak planar cavity with the surface of the sample.

Experimental Setup: The sample is placed inside an exchange-gas dipstick located in a liquid-helium bath resulting in a constant temperature of 4.2 K. Optical access is granted from the top using a state-of-the art cross-polarized resonance fluorescence confocal microscope.[40] High-precision positioning of the QD with respect to the laser field is achieved via a stack of nanopositioners. For excitation, a 150 fs Ti:Sapph laser is used whose output is split into two pulses and shaped using two fully independent 4 f pulse-shapers.[41] Full control of the sub-picosecond time delay between the two pulses is achieved by a delay line. Simultaneously, two separate optical attenuators allow independent control of the pulse area of both pulses after which the pulses are recombined and sent to the confocal microscope. This experimental setup enables to individually control frequency, pulse duration and intensity of the two pulses and their relative time delay. The emitted photons are frequency filtered and detected by either a spectrometer and a CCD camera or by single-photon avalanche diodes (SPADs).

Note added: During the review process of this manuscript a related work by Joos et al.[42] was published.

Supporting Information

Supporting Information is available from the Wiley Online Library or from the author.

Acknowledgements

K.B., F.S., and S.K.K. contributed equally to this work. The authors gratefully acknowledge financial support from the German Federal Ministry of Education and Research via the funding program Photonics Research Germany (Contract No. 13N14846), the European Union's Horizon 2020 research and innovation program under Grants Agreement No. 862035 (QLUSTER) and No. 899814 (Qurope), the Deutsche Forschungsgemeinschaft (DFG, German Research Foundation) via the projects MQCL (INST 95/1220-1), CNLG (MU 4215/4-1), TRR 142 (Grant No. 231447078), and Germany's Excellence Strategy (MCQST, EXC-2111, 390814868), the TUM Institute for Advanced Study, the Bavarian State Ministry of Science and Arts via the project EQAP and the Exploring Quantum Matter (ExQM) program funded by the state of Bavaria.

Open access funding enabled and organized by Projekt DEAL.

Conflict of Interest

The authors declare no conflict of interest.

Data Availability Statement

The data that support the findings of this study are available from the corresponding author upon reasonable request.

Keywords

coherent excitation, semiconductor quantum dot, swing-up excitation technique, two-level system

Received: October 15, 2023
Revised: December 22, 2023
Published online: January 28, 2024

[1] P. Senellart, G. Solomon, A. White, *Nat. Nanotechnol.* **2017**, *12*, 1026.
[2] W. B. Gao, P. Fallahi, E. Togan, J. Miguel-Sanchez, A. Imamoglu, *Nature* **2012**, *491*, 426.
[3] S. Sun, H. Kim, G. S. Solomon, E. Waks, *Nat. Nanotechnol.* **2016**, *11*, 539.
[4] A. Delteil, Z. Sun, W.-b. Gao, E. Togan, S. Faelt, A. Imamoğlu, *Nat. Phys.* **2016**, *12*, 218.
[5] R. Stockill, M. J. Stanley, L. Huthmacher, E. Clarke, M. Hugues, A. J. Miller, C. Matthiesen, C. Le Gall, M. Atatüre, *Phys. Rev. Lett.* **2017**, *119*, 010503.
[6] I. Schwartz, D. Cogan, E. R. Schmidgall, Y. Don, L. Gantz, O. Kenneth, N. H. Lindner, D. Gershoni, *Science* **2016**, *354*, 434.
[7] D. Istrati, Y. Pilnyak, J. C. Loredo, C. Antón, N. Somaschi, P. Hilaire, H. Ollivier, M. Esmann, L. Cohen, L. Vidro, C. Millet, A. Lemaître, I. Sagnes, A. Harouri, L. Lanco, P. Senellart, H. S. Eisenberg, *Nat. Commun.* **2020**, *11*, 5501.
[8] E. Moreau, I. Robert, J. Gérard, I. Abram, L. Manin, V. Thierry-Mieg, *Appl. Phys. Lett.* **2001**, *79*, 2865.
[9] C. Santori, D. Fattal, J. Vučković, G. S. Solomon, Y. Yamamoto, *Nature* **2002**, *419*, 594.
[10] O. Gazzano, S. Michaelis de Vasconcellos, C. Arnold, A. Nowak, E. Galopin, I. Sagnes, L. Lanco, A. Lemaître, P. Senellart, *Nat. Commun.* **2013**, *4*, 1425.
[11] L. Schweickert, K. D. Jöns, K. D. Zeuner, S. F. Covre Da Silva, H. Huang, T. Lettner, M. Reindl, J. Zichi, R. Trotta, A. Rastelli, V. Zwiller, *Appl. Phys. Lett.* **2018**, *112*, 093106.
[12] N. Tomm, A. Javadi, N. O. Antoniadis, D. Najer, M. C. Löbl, A. R. Korsch, R. Schott, S. R. Valentin, A. D. Wieck, A. Ludwig, R. J. Warburton, *Nat. Nanotechnol.* **2021**, *16*, 399.
[13] Y.-M. He, Y. He, Y.-J. Wei, D. Wu, M. Atatüre, C. Schneider, S. Höfling, M. Kamp, C.-Y. Lu, J.-W. Pan, *Nat. Nanotechnol.* **2013**, *8*, 213.
[14] A. V. Kuhlmann, J. H. Prechtel, J. Houel, A. Ludwig, D. Reuter, A. D. Wieck, R. J. Warburton, *Nat. Commun.* **2015**, *6*, 8204.
[15] P.-L. Ardelt, L. Hanschke, K. A. Fischer, K. Müller, A. Kleinkauf, M. Koller, A. Bechtold, T. Simmet, J. Wierzbowski, H. Riedl, G. Abstreiter, J. J. Finley, *Phys. Rev. B* **2014**, *90*, 241404.
[16] M. Reindl, J. H. Weber, D. Huber, C. Schimpf, S. F. Covre da Silva, S. L. Portalupi, R. Trotta, P. Michler, A. Rastelli, *Phys. Rev. B* **2019**, *100*, 155420.
[17] S. E. Thomas, M. Billard, N. Coste, S. C. Wein, Priya, H. Ollivier, O. Krebs, L. Tazaïrt, A. Harouri, A. Lemaitre, I. Sagnes, C. Anton, L. Lanco, N. Somaschi, J. C. Loredo, P. Senellart, *Phys. Rev. Lett.* **2021**, *126*, 233601.
[18] M. E. Ware, E. A. Stinaff, D. Gammon, M. F. Doty, A. S. Bracker, D. Gershoni, V. L. Korenev, i. m. c. C. Bădescu, Y. Lyanda-Geller, T. L. Reinecke, *Phys. Rev. Lett.* **2005**, *95*, 177403.
[19] D. Cogan, Z. E. Su, O. Kenneth, D. Gershoni, *Nat. Photonics* **2023**, *17*, 324.
[20] Y.-M. He, H. Wang, C. Wang, M.-C. Chen, X. Ding, J. Qin, Z.-C. Duan, S. Chen, J.-P. Li, R.-Z. Liu, C. Schneider, M. Atatüre, S. Höfling, C.-Y. Lu, J.-W. Pan, *Nat. Phys.* **2019**, *15*, 941.

[21] Z. X. Koong, E. Scerri, M. Rambach, M. Cygorek, M. Brotons-Gisbert, R. Picard, Y. Ma, S. I. Park, J. D. Song, E. M. Gauger, B. D. Gerardot, *Phys. Rev. Lett.* **2021**, *126*, 047403.
[22] K. Brunner, G. Abstreiter, G. Böhm, G. Tränkle, G. Weimann, *Phys. Rev. Lett.* **1994**, *73*, 1138.
[23] L. Hanschke, K. A. Fischer, S. Appel, D. Lukin, J. Wierzbowski, S. Sun, R. Trivedi, J. Vučković, J. J. Finley, K. Müller, *npj Quantum Inf.* **2018**, *4*, 43.
[24] A. Nick Vamivakas, Y. Zhao, C.-Y. Lu, M. Atatüre, *Nat. Phys.* **2009**, *5*, 198.
[25] E. B. Flagg, A. Muller, J. Robertson, S. Founta, D. Deppe, M. Xiao, W. Ma, G. Salamo, C.-K. Shih, *Nat. Phys.* **2009**, *5*, 203.
[26] A. Muller, E. B. Flagg, P. Bianucci, X. Y. Wang, D. G. Deppe, W. Ma, J. Zhang, G. J. Salamo, M. Xiao, C. K. Shih, *Phys. Rev. Lett.* **2007**, *99*, 187402.
[27] C. Simon, J.-P. Poizat, *Phys. Rev. Lett.* **2005**, *94*, 030502.
[28] T. Huber, A. Predojević, H. Zoubi, H. Jayakumar, G. S. Solomon, G. Weihs, *Opt. Express* **2013**, *21*, 9890.
[29] F. Sbresny, L. Hanschke, E. Schöll, W. Rauhaus, B. Scaparra, K. Boos, E. Zubizarreta Casalengua, H. Riedl, E. del Valle, J. J. Finley, K. D. Jöns, K. Müller, *Phys. Rev. Lett.* **2022**, *128*, 093603.
[30] T. K. Bracht, M. Cosacchi, T. Seidelmann, M. Cygorek, A. Vagov, V. M. Axt, T. Heindel, D. E. Reiter, *PRX Quantum* **2021**, *2*, 040354.
[31] Y. Karli, F. Kappe, V. Remesh, T. K. Bracht, J. Münzberg, S. Covre da Silva, T. Seidelmann, V. M. Axt, A. Rastelli, D. E. Reiter, G. Weihs, *Nano Lett.* **2022**, *22*, 6567.
[32] T. Stievater, X. Li, D. G. Steel, D. Gammon, D. Katzer, D. Park, C. Piermarocchi, L. Sham, *Phys. Rev. Lett.* **2001**, *87*, 133603.
[33] See Supporting Information.
[34] T. K. Bracht, T. Seidelmann, Y. Karli, F. Kappe, V. Remesh, G. Weihs, V. M. Axt, D. E. Reiter, *Phys. Rev. B* **2023**, *107*, 035425.
[35] R. J. Warburton, C. Schäflein, D. Haft, F. Bickel, A. Lorke, K. Karrai, J. M. Garcia, W. Schoenfeld, P. M. Petroff, *Nature* **2000**, *405*, 926.
[36] S. Seidl, M. Kroner, P. A. Dalgarno, A. Högele, J. M. Smith, M. Ediger, B. D. Gerardot, J. M. Garcia, P. M. Petroff, K. Karrai, R. J. Warburton, *Phys. Rev. B* **2005**, *72*, 195339.
[37] K. A. Fischer, L. Hanschke, M. Kremser, J. J. Finley, K. Müller, J. Vučković, *Quantum Sci. Technol.* **2018**, *3*, 014006.
[38] J. Loredo, C. Antón, B. Reznychenko, P. Hilaire, A. Harouri, C. Millet, H. Ollivier, N. Somaschi, L. De Santis, A. Lemaître, I. Sagnes, L. Lanco, A. Auffèves, O. Krebs, P. Senellart, *Nat. Photonics* **2019**, *13*, 803.
[39] M. Davanco, M. T. Rakher, W. Wegscheider, D. Schuh, A. Badolato, K. Srinivasan, *Appl. Phys. Lett.* **2011**, *99*, 12.
[40] A. V. Kuhlmann, J. Houel, A. Ludwig, L. Greuter, D. Reuter, A. D. Wieck, M. Poggio, R. J. Warburton, *Nat. Phys.* **2013**, *9*, 570.
[41] A. M. Weiner, J. P. Heritage, E. M. Kirschner, *J. Opt. Soc. Am. B* **1988**, *5*, 1563.
[42] R. Joos, S. Bauer, C. Rupp, S. Kolatschek, W. Fischer, C. Nawrath, P. Vijayan, R. Sittig, M. Jetter, S. L. Portalupi, P. Michler, preprint arXiv:2310.20647 **2023**.